Nanocomposite MFI-alumina membranes via pore-plugging synthesis: Genesis of the zeolite material

Y. Li[1,2], M. Pera-Titus[1], G. Xiong[2], W. Yang[2], E. Landrivon[1], S. Miachon[1,*] & J.-A. Dalmon[1]

[1]*Institut de Recherches sur la Catalyse et l'Environnement de Lyon (IRCELYON), UMR 5256 CNRS - Université de Lyon,*
2, av. A. Einstein, 69626 Villeurbanne cedex, France
[2]*Dalian Institute of Chemical Physics, Chinese Academy of Sciences, Dalian 116023, China*

Revised version from 14 September 2008

This paper presents a study of MFI-type zeolite crystal growth during hydrothermal synthesis of nanocomposite MFI-alumina membranes by the pore-plugging method, using the standard protocol described in a previous study (S. Miachon et al., *J. Membr. Sci.* **2006**, *281*, 228). To this aim, the materials have been characterized by SEM, EDX, pure H_2 gas permeance and *n*-butane/H_2 mixture separation at different stages of the synthesis. The effect of synthesis time in the range 4-89 h and the effect of a 9-h interruption after a 8-h hydrothermal synthesis have been surveyed, as well as the mean pore size and the alumina phase of the support inner layer. Our results suggest that an interruption during the synthesis is necessary to allow the zeolite precursor to diffuse into the support pores. This diffusion leads to a further growth of zeolite crystals into the support matrix without formation of a continuous zeolite film on top of the support, as is usually reported in the literature. The zeolite crystals are fully embedded into the support top layer after at least 53-h synthesis time, leading to high quality membranes in only one synthesis run. The nanocomposite MFI-alumina architecture at the nanoscale has important consequences in improving the gas separation performance of this kind of materials when compared to more conventional film-like structures. A method based on gas transport measurements has been used to determine the effective thickness of the separating material.

Keywords: MFI zeolite, membrane, nanocomposite, film, mass transfer

1 Introduction

Since the mid 90s, much work has been done in the field of zeolite membranes for gas separation and pervaporation applications, as reported in several reviews [1-7]. Recently, A-type zeolite membranes have been implemented at the industrial scale for pervaporation dehydration applications [8]. The challenge is to prepare realistic membrane surface areas whose properties only depend on the intrinsic properties of zeolites. In fact, the membrane performance is determined by the quality and intergrowth of the zeolite material coating the porous support, whose thickness must be as low as possible to favour high permeances. Moreover, besides intercrystaline defects, the density and nature of grain boundaries may also affect the permeation and separation performance of the membranes [9-11].

MFI-type zeolite membranes have often been the target of the investigations for gas separation applications due to their small pore sizes (~0.5 nm) and mild crystallization conditions [7]. Most often, the studies have focused on the synthesis of continuous and well-intergrown thin films on top of a porous support that ensures mechanical resistance. Zeolite films can be prepared by either *in situ* or seeded hydrothermal synthesis, or by dry-gel conversion methods [6]. Specific zeolite crystal orientation in the layers can be also achieved by fine-tuning the seed characteristics (size, shape, concentration) prior to hydrothermal synthesis [12,13], which might influence the gas transport properties [14]. The main shortcoming of this configuration is the thermal expansion mismatch between the support and the zeolite layer, which can lead to crack formation during calcination and further cooling [4,7], or to intercrystalline opening when operated at elevated temperatures (>400 K), depending on the crystal size [15].

In previous studies [16-19], some of us have reported on the synthesis and improved gas permeation and separation performance of nanocomposite MFI – alumina membranes (prepared either as tubes or hollow fibres) to overcome these limitations. In this architecture, compared to a film, the active phase is embedded into the host ceramic alumina porous network via pore-plugging hydrothermal synthesis. Detailed transmission electron micrographs have revealed that zeolite crystals plug neighbouring support pores [16], which confers to the material higher resistance to long-range thermal stresses commonly observed in supported zeolite films [20-22]. Another consequence is that mass transfer within these membranes at high temperature is kept governed by zeolite pores instead of intercrystalline openings that may appear in film-like configurations.

Nanocomposite membranes have shown high potential in several separation applications (e.g., xylene isomer separation [23] and ammonia recovery [24]), and combined with a catalyst in membrane reactors (e.g., isobutane dehydrogenation [25] and xylene isomerization [23]). Besides, this nanocomposite configuration has also been applied to the synthesis of other membrane materials, such as Pd-ceramic [26] and

---

* Corresponding author. Tel: +33 (0) 472 44 53 84,
Fax: +33 (0) 472445399, sylvain.miachon@ircelyon.univ-lyon1.fr

MCM-41 'LUS' [27] membranes, these latter showing high membrane quality together with high gas and water permeation performance and high structural stability.

In a previous study [16], the composition of the precursor solution and the support pore size were shown to play a crucial role on the final membrane quality. An optimum on membrane quality is obtained using a TPAOH/Si molar ratio of 0.45, corresponding to [TPAOH] = 0.9 mol/l. This concentration, when compared to others, involves a lower proportion of Q^3, and a higher proportion of Q^2 oligomers(*), long enough to favour zeolite crystallization, but at the same time short enough to diffuse into the support pores. This has been inferred from ^{29}Si NMR analysis. Light absorption analysis of the precursor also showed a strong influence of the precursor concentration on precursor size. Moreover, the introduction of a heating interruption during hydrothermal synthesis leads to higher membrane separation performance. However, no detailed study has been published to date reporting on the effect of this interruption on the MFI zeolite crystal growth mechanism. This paper is therefore devoted to gain insight into this aspect, as a follow-up to two previous articles devoted to this type of membranes [15,16]. In this third contribution, our research strategy has focused on the analysis of the effect of the two main variables addressed in ref. [16]: (1) the synthesis time in the range 4-89 h, including a 9-h interruption after 8 h, and (2) the pore size and alumina phase of the support top layer.

Moreover, on conventional film-like structured materials, the membrane thickness is usually deduced from film thickness as measured from SEM imaging [1,7]. In nanocomposite materials, however, microscopy techniques cannot be applied, since no film is formed. Accordingly, a specific method based on mass transport measurements is proposed here to determine the effective thickness. This is the thickness of closed material corresponding to the real mass transfer resistance during operation, and responsible for the selectivity.

2 Experimental

2.1 Membrane supports

The membranes were prepared on porous asymmetric 15-cm long tubular supports with 7 mm i.d. and 10 mm o.d. provided by Pall Exekia (Membralox T1-70). The quality of the supports was deduced from the values of the first bubble point pressure, higher than 80 kPa in all cases. Two of these supports consisted of three α-alumina layers with mean pore size and thickness decreasing from the outer to the inner side of the tube, with the following pore size sequences (as given by the tube provider): 12-0.8-0.2 μm and 12-0.8-0.1 μm (top-layer thickness: 10 μm in both cases). The first 12-μm layer had a porosity of 33%, whereas that of the other two was 30%. Moreover, a third support, also supplied by Pall-Exekia, was also used, which consisted of a three-layered α-alumina tube (0.2-μm-mean-pore-size of the last layer) with a fourth 5-nm γ-alumina top layer deposited on the inner surface of the tube.

In all cases, both ends of the supports were enamelled (1 cm at each side) for sealing purposes, defining a permeation length of 15 cm and an active surface of 28.6 cm^2.

2.2 Hydrothermal synthesis

The nanocomposite MFI-alumina membranes were prepared by *in situ* hydrothermal synthesis using the pore-plugging method as described in previous studies [16,17]. Shortly, a clear solution containing a molar composition of 1.0 SiO_2 : 0.45 TPAOH : 27.8 H_2O was matured for 72 h. The support tube was soaked in the solution placed in a Teflon-lined autoclave. The closed autoclave was then placed vertically in an oven preheated at 170°C. The standard temperature program is depicted in Fig. 1. It included a 9-h interruption after 8 h synthesis, its total duration being 89 h. In order to follow the growth of the nanocomposite material, some syntheses were stopped after different times (see Fig. 1) and the corresponding materials were then characterised by gas transport and other techniques. In each case, some support slices were added to the autoclave on top of the tube during the syntheses for further electron microscopy analysis.

After the synthesis, the autoclave was cooled down to room temperature, the synthesized membranes were removed, washed with deionised water until pH neutrality, and dried overnight at room temperature and subsequently at 120°C for 12 h. A membrane integrity test (N_2 permeation under 400 mbar differential pressure) was performed at this stage to assess for the presence of large defects or cracks. The dried membranes were then calcined at 500°C for 8 h under air stream for template removal.

The tube weight was measured before synthesis, after the drying step and after calcination, the samples being kept under dry atmosphere in all the measurements.

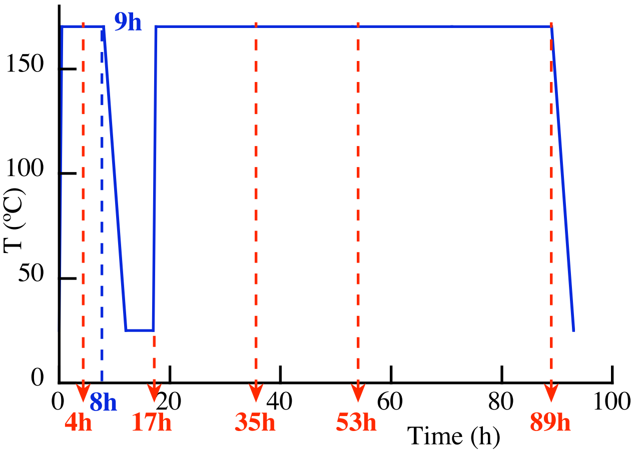

Fig. 1. Standard temperature program during synthesis, including a 9-h interruption after 8 h synthesis. Material samples were analysed after the times indicated by the dotted line arrows on bottom (4-89 h).

2.3 Membrane characterization

2.3.1 Electron microscopy characterization

Scanning electron microscopy (SEM) images on membrane tube slices were obtained using a Philips-XL-30 microscope at 20 kV equipped with EDS analysis (EDAX-phoenix).

2.3.2 Pure H_2 and alkane permeation and n-butane/H_2 separation

Prior to any gas permeance or separation measurement, the membranes were set in a tubular stainless steel module and each end sealed using graphite cylindrical o-rings (Cefilac-Fargraf) and submitted to desorption conditions. This was

---

(*) Q^n is a notation referring to the number *n* of siloxane bridges around a Si atom (the other being –OH groups). Larger *n* values are usually associated with larger oligomer particles.

achieved by pre-treatment at 400°C for 6 h under N_2 flow (20 NmL.min^{-1}) at both retentate and permeate sides with a heating ramp of 1°C.min^{-1}. After a 6-h plateau, the temperature was reduced to the room value in ca. 3 h. The purpose of this step was to remove adsorbed species, such as water coming from air humidity when the sample is exposed to open atmosphere, or gases adsorbed in previous experiments. Further details about this and other pre-treatment protocols can be found in ref. [29].

Pure hydrogen, methane, ethane, propane and *n*-butane permeation experiments were performed at room temperature in dead-end mode. The target gas was fed to the retentate side of the membrane at 120 to 200 kPa, while the permeate side was kept at atmospheric pressure. The gas permeance, Π (μmol.m^{-2}.s^{-1}.Pa^{-1}), was measured using a bubble flowmeter, connected to the permeate stream of the membrane. The evolution of the pure gas permeance of the alkanes with temperature was used to infer the value of the effective thickness of the zeolitic material in the nanocomposite membranes.

The *n*-butane/H_2 mixture separation tests were performed in Wicke-Kallenbach conditions. The pressure at both sides of the module was kept at 120 kPa, with no pressure drop. The mixture was fed to the inner side of the membrane using N_2 as carrier gas. The flow rate of each gas was measured using mass flow controllers (Brooks 5850TR and 5850E) and was kept at 55 NmL·min^{-1} for N_2 and 11 NmL·min^{-1} for both n-butane and H_2 in the feed side of the membrane. In the permeate side, N_2 was also used as sweep gas at (52 NmL·min^{-1}) in counter-current flow.

The composition at the feed, retentate and permeate streams was analyzed by a HP 5890/series II Gas Chromatograph equipped with a Porapak Q column and FID and TCD detectors. The separation factor of *n*-butane over H_2, $Sf_{C4H10/H2}$, was calculated as the permeate-to-feed composition ratio of *n*-butane, divided by the same ratio for H_2. The separation factor was measured at steady state and room temperature. Over a certain value, due to the very low amount of hydrogen in the permeate, the separation factor scale should be regarded as more logarithmic than linear.

3 Results

3.1 Material evolution as a function of synthesis time

3.1.1 Weight uptake and membrane integrity test

Table 1 summarizes the main results obtained for the weight uptake and pure N_2 permeance before calcination (membrane integrity test) during the genesis of MFI-alumina membranes. After a sharp increase during the first 4 h, the weight uptake increases progressively during the synthesis of the MFI material. At the same time, the N_2 permeance before calcination is drastically reduced after 35 h synthesis, suggesting an efficient pore plugging.

3.1.2 Morphology of MFI-alumina membranes

Fig. 2 shows the cross-section SEM micrographs of the last 2 layers (0.8 and 0.2 μm pore size, respectively) of an α-alumina support (Fig. 2a), and of the as-synthesized tube slices after calcination for different synthesis times according to the temperature program depicted in Fig. 1 (Figs. 2b-f). Fig. 3b suggests the nucleation of zeolite seeds on the surface and into the support pores of the 0.2-μm top layer after 4-h synthesis. In the following images (Figs. 2c-f), progressive changes in morphology are visible, leading to the final situation (Fig. 2f), where zeolitic material is present within the last support layer, without formation of a continuous zeolite film on top.

Table 1.
Nitrogen permeance before calcination (second column) and weight uptake (third column) of the nanocomposite MFI-alumina membranes synthesized on 0.2-μm top layer supports, as a function of synthesis time.

Time [h]	Π_{N2} (before calcination) [μmol·m^{-2}·s^{-1}·Pa^{-1}]	wt.% MFI (after calcination)
4	0.13	1.03
17	0.03	1.45
35	$<10^{-4}$	1.94
53	$<10^{-4}$	2.24
89	$<10^{-4}$	2.72
200	$<10^{-4}$	3.15

3.1.3 Evolution of the Si/Al ratio across the membrane thickness

Fig. 3 shows the qualitative evolution, as a function of the synthesis time, of the Si/Al ratio trend measured by EDX along the radial direction and from the inner surface of the membrane tube. The analyses were carried out after synthesis on 0.2-μm top-layer supports with spots of about 2 x 2 μm^2, larger than the mean pore size of the last two layers (0.8 and 0.2 μm, respectively). Therefore, these measurements provide a comparison estimate of the amount of MFI material embedded in the support porous network. It is to be noted that, due to the nature of the material (roughness, nanocomposite architecture…), the Si/Al ratios were obtained following semi-quantitative analysis.

Fig. 3 also shows that the Si/Al ratio at each support depth increases with hydrothermal synthesis time. In particular, after 4 and 17-h hydrothermal synthesis time, the Si/Al ratio on the inner tube surface is higher than in the depth of the material. In contrast, after 53 h, the Si/Al ratio within the support pores becomes higher than on the inner tube surface, with a maximum value at about 20 μm. This trend is preserved after 89-h hydrothermal synthesis, the Si/Al ratio now showing higher values all along the depth than on the inner tube surface.

3.1.4 Evolution of pure H_2 permeance and n-butane/H_2 separation factor with synthesis time

Fig. 4 shows the evolution of the weight uptake, room-temperature pure H_2 permeance and *n*-butane/H_2 separation factor (taken as membrane quality estimate) during synthesis on different membranes prepared on 0.2-μm-top-layer-support (each data point represents an average of different samples). As can be seen, the MFI weight uptake increases monotonically during the synthesis, from 0.18 g after 4 h to 0.43 g after 89 h, corresponding to a tube weight change ranging from 1.1 to 2.6 wt.% (or from 6 to 15 mgMFI/cm^2 of tube). As expected, the increasing MFI weight uptake is accompanied by a reduction of the pure H_2 permeance, from 0.55 to 0.25 μm.m^{-2}.s^{-1}.Pa^{-1}, and by a net raise of the *n*-butane/H_2 separation factor, from 1 to about 100 (the latter value corresponding to the mean performance of a large series of these materials including the values listed in Table 1).

It is noteworthy that, when increasing the synthesis time from 89 to 200 h (not shown), although the n-butane/H_2 separation factor is not enhanced, the weight uptake goes on increasing and the pure H_2 permeance shows some reduction.

Also, interrupting the synthesis after 4 h instead of 8 h, high separation factors (up to 155) are still obtained.

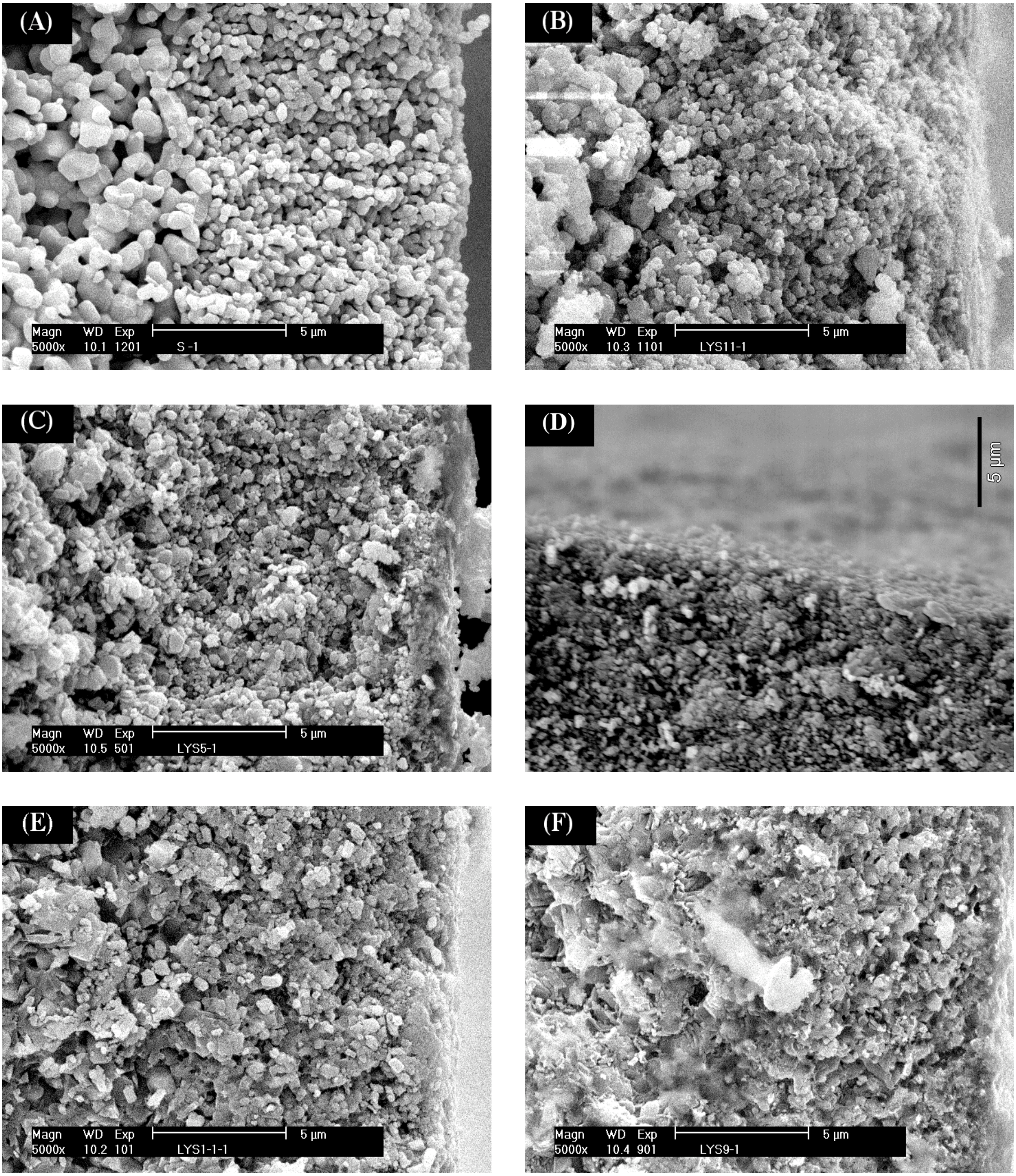

Fig. 2. Cross-section SEM micrographs of membrane tube slices made on support including a top layer of 0.2 µm mean pore size subjected to hydrothermal synthesis for different synthesis times. (A) support, (B) 4 h, (C) 17 h, (D) 35 h, (E) 53 h, (F) 89 h.

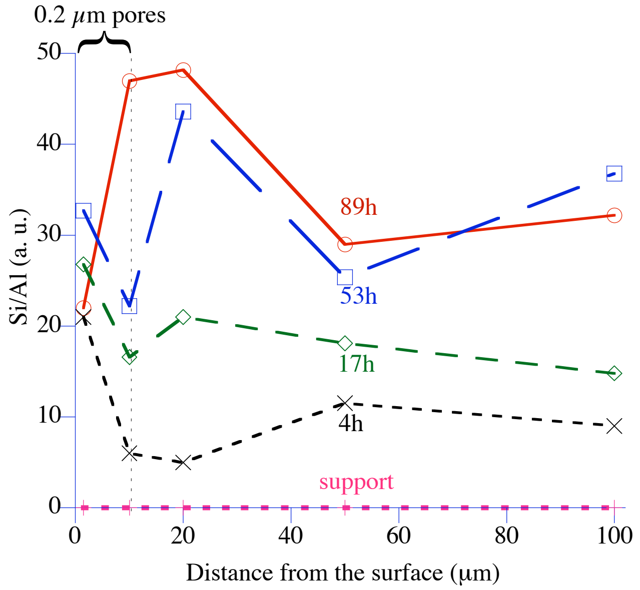

Fig. 3. Comparison of qualitative trends of Si/Al ratios (expressed from EDX semi-quantitative analyses), as a function of the distance from the inner surface of membrane tubes made on supports of 0.2-µm pore size top layer for different synthesis types.

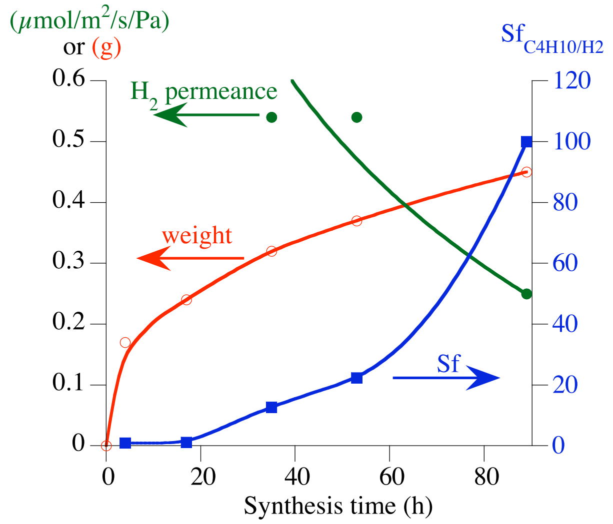

Fig. 4. Tube weight uptake, room temperature pure H_2 permeance and *n*-butane/H_2 separation factor (Sf) as a function of synthesis time for membranes prepared on 0.2-µm top-layer supports. Hydrogen permeance values are very high at lower synthesis times (not shown).

3.1.5 *Influence of top-layer characteristics*

Table 2 summarizes the main results obtained for the weight uptake, pure H_2 permeance and *n*-butane/H_2 separation factors of the synthesized MFI-alumina membranes after 89 h as a function of the mean pore size and nature of the support top layer. As can be seen, for both 0.1 and 0.2-µm α-alumina top-layer supports, the sample uptake after synthesis lies in a narrow range (2.7-3.0 wt.% or 15-18 mgMFI/cm^2 of tube). In the case of tubes including an additional γ-alumina 5-nm mean-pore size layer, the weight uptake shows values in a close range, but seem more disperse. Although all the membranes display similar pure H_2 permeance, those prepared on 5-nm γ-alumina supports show lower *n*-butane/H_2 separation factors.

Fig. 5 shows the temperature evolution of the *n*-butane/H_2 separation factor for three membranes synthesized on 0.1 and 0.2-µm-top-layer supports (membranes MFI01-1, MFI01-2 and MFI02-1 in Table 1). As can be seen, for all the membranes, the *n*-butane/H_2 separation factor decreases monotonically with increasing temperature.

Some SEM micrographs of the 5-nm-pore-size γ-alumina tubes before and after MFI synthesis are shown in Fig. 6. A strong change in the material morphology occurs during zeolite synthesis: large cracks appear in the γ-alumina layer (see Fig. 6c), including its removal in some areas (Fig. 6b). In these zones (Fig. 6d), very few zeolite crystals have grown perpendicularly to the α-alumina support surface. On the remaining γ-alumina surface, non-connected zeolite crystals can be visualized in some zones, with a variable population density (Fig. 6c).

Table 2.
Weight uptake, pure H_2 permeance (Π_{H2}) and *n*-butane/H_2 separation factor ($Sf_{C4H10/H2}$) of the nanocomposite MFI-alumina zeolite membranes synthesized in this study after 89 h and subjected to an interruption during the synthesis.

Top-layer pore size	Membrane reference	wt.% MFI	Π_{H2} [µmol·m^{-2}·s^{-1}·Pa^{-1}]	$Sf_{C4H10/H2}$ [-]
0.2 µm	MFI02-1	2.7	0.26	350
	MFI02-2	2.8	0.24	33
0.1 µm	MFI01-1	-	0.34	151
	MFI01-2	-	0.25	454
	MFI01-3	2.8	0.36	∞
	MFI01-4	2.7	0.49	98
	MFI01-5	3.0	0.22	28
	MFI01-6	2.8	-	-
5 nm	MFI5-1	4.3	0.37	2
	MFI5-2	3.1	0.50	5
	MFI5-3	2.8	0.27	2

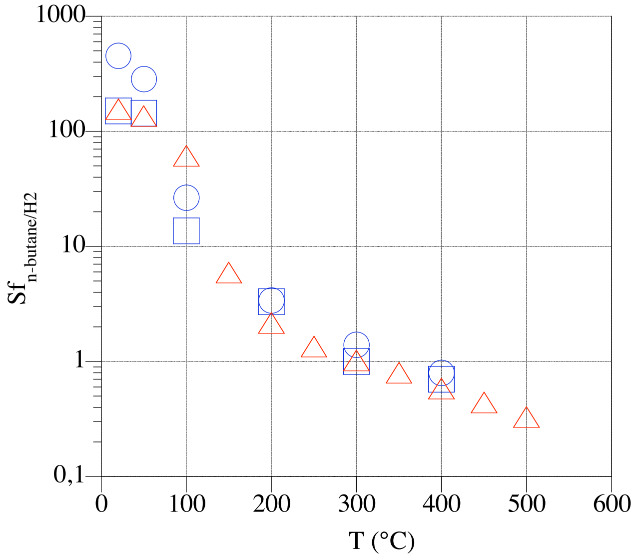

Fig. 5. Evolution of n-butane/H_2 separation factor ($Sf_{n\text{-}butane/H2}$) with temperature for membrane MFI01-1 (cycles) and MFI01-2 (squares) prepared on a 0.1-µm toplayer support, and membrane MFI02-1 (triangles) prepared on a 0.2 µm support. Data was obtained after high temperature treatment (400°C for 6 hours).

3.2 *Effective thickness measurement*

The thermal behaviour of pure gas permeance can be used to deduce the effective thickness of the synthesized nanocomposite membranes. As was presented in an earlier study [15], nanocomposite MFI-alumina membranes offer a permeation thermal behaviour that can be well fitted to an equation directly deduced from the Maxwell-Stefan (MS) theory:

$$N = \frac{c_{sat}\rho\varepsilon D_o^{\infty}}{\tau\ell}\ln\left[\frac{1+\frac{P_R}{P^o}\exp\left(\frac{\Delta S^o_{ads}-R}{R}-\frac{\Delta H^o_{ads}}{RT}\right)}{1+\frac{P_P}{P^o}\exp\left(\frac{\Delta S^o_{ads}-R}{R}-\frac{\Delta H^o_{ads}}{RT}\right)}\right]\exp\left[-\frac{E_D}{RT}\right] \qquad (1)$$

with the parameter values taken from [15].

In this work, we use the fittings of this model to the permeation-temperature plot for a series of pure linear alkane (C1-C4), since for these gases sufficient adsorption and diffusion data are available in the literature. Contrarily to the approach of our previous study [15], where the thickness of the zeolite material was arbitrarily chosen, we present here the results of the fitted parameters expressed as D_o^{∞}/ℓ ratio (see Table 3).

The D_o^{∞}/ℓ ratio decreases sharply with the chain length of the alkane. This reflects a reduction of the diffusivity of the alkane, ℓ being constant. As will be shown below, this is the principle of the measurement..

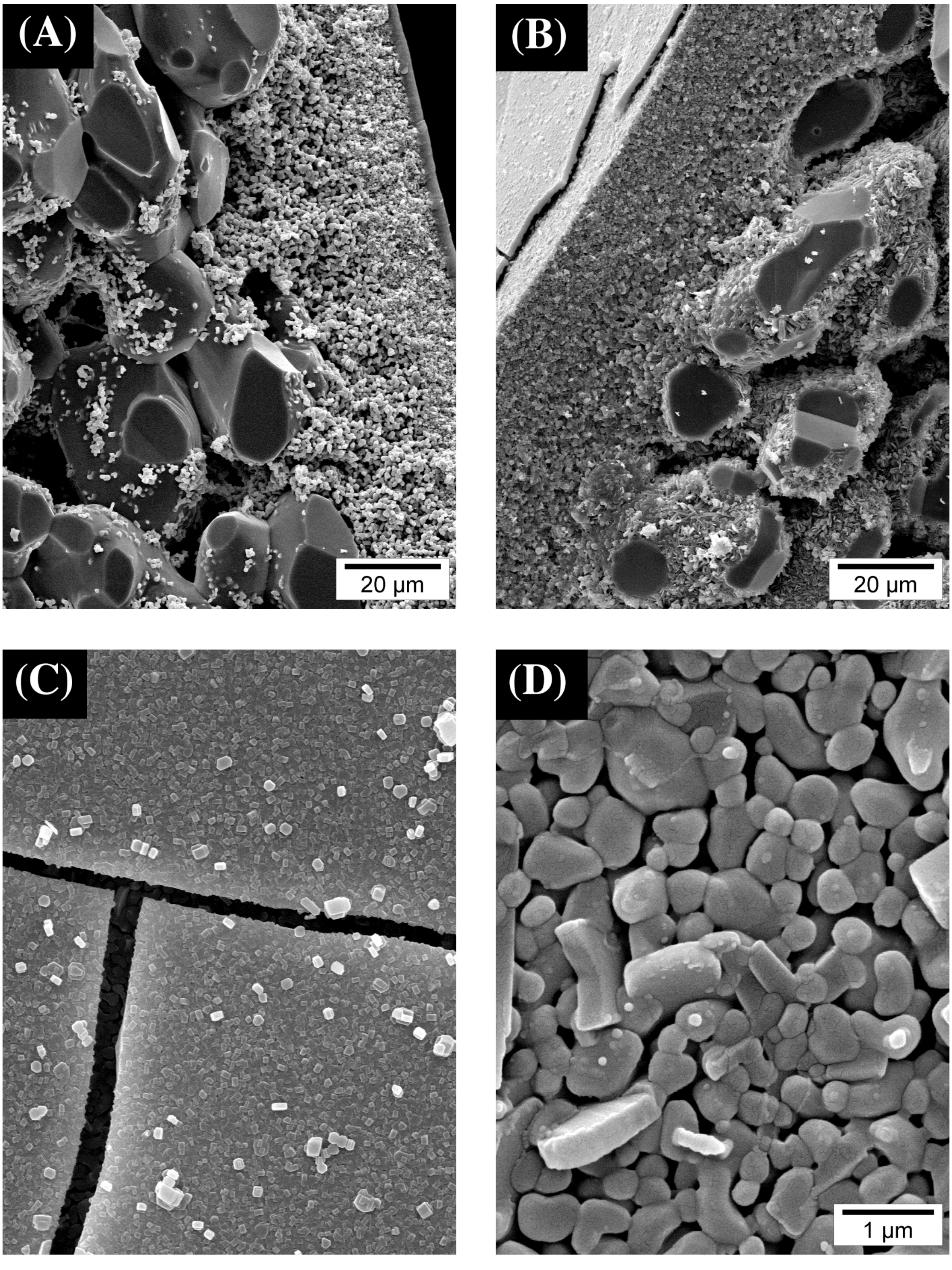

Fig. 6. SEM micrograph of a cross-section view of a 5-nm mean-pore size γ-alumina fresh support (A). SEM views of the same material after 89-h synthesis: (B) cross-section view, (C) top-view of the remaining γ-alumina, and (D) top-view of a liberated α-alumina top-layer surface.

4 Discussion

4.1 Synthesis kinetics of nanocomposite MFI-alumina membranes

The kinetics of MFI synthesis can be studied by inspecting the curve of weight uptake in Fig. 4. The amount of zeolite precursor present in the porous matrix in the beginning of the crystallization (≈0.24 g of SiO_2 corresponding to about 2 mL solution) is rapidly consumed in a first step. This could be attributed to the nucleation process. Zeolite nucleation can be promoted by the presence of Al leached from the support [9,16,30]. Further on, the tube weight uptake is progressively slowed down due to nutrient depletion in the porous network, which limits the crystal growth. As a matter of fact, one can observe that, just after the interruption (17-h sample), the weight uptake matches the total amount of zeolite precursor initially available in the porous matrix. This could correspond to a mechanism where the precursor diffusion from the bulk solution into the porous system is slower than zeolite synthesis

Table 3.
Fitted parameter ($D_\circ^\infty/\ell$) from MS modelling (Eq. 1) for four hydrocarbons.

Gas	$D_\circ^\infty/\ell$ [mm.s^{-1}]
CH_4	101 ± 7
C_2H_6	20.7 ± 0.9
C_3H_8	11.5 ± 0.8
n-C_4H_{10}	6.7 ± 0.4

During an interruption, the reduction of temperature inhibits nucleation and crystal growth processes. However, molecular diffusion processes are only slightly affected by temperature. During this time, an increase of precursor concentration in the porous network is therefore expected to occur by diffusion. This increase in concentration might favour further crystal growth inside the pores when the synthesis is resumed, improving in its turn the pore plugging during subsequent hydrothermal synthesis at 170°C. As the kinetics of crystal growth is expected to be slower than the initial nucleation, this might translate into a sustained increase of the weight uptake (see Fig. 4). From 17 h to the end of the synthesis (i.e. 89 h), the tube weight uptake matches again the amount of precursor present in the porous volume.

Note that without an interruption, one should expect that crystallization would be favoured in the precursor-rich areas surrounding the bulk of the solution. Moreover, in absence of the interruption, the support top layer would hinder precursor diffusion, avoiding its access into the support pores. This could promote the growth of a film on top of the support, as is generally observed in most of the reported studies using *in situ* hydrothermal synthesis. In fact, a theoretical thickness value of 30 μm might be obtained if the whole zeolite weight uptake were ascribed to film formation, a picture that is in complete disagreement with the SEM micrographs shown in Fig. 2.

A general scheme of the nanocomposite genesis on a typical alumina support is given in Fig. 7. The likelihood that MFI crystals plug the pores is inversely proportional to their pore size. In other words, it is more likely that zeolite crystals plug the 0.2-μm top layer instead of the other two of the support (i.e. 0.8 and 12 μm, respectively).

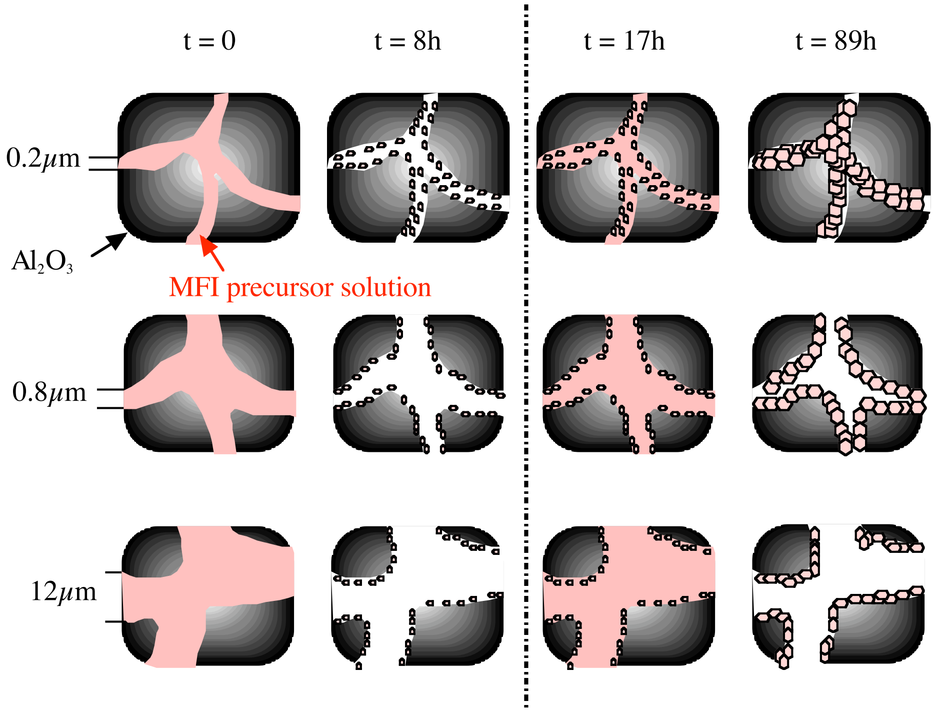

Fig. 7. Scheme of the genesis of nanocomposite membranes on a typical 3-layer α-alumina support. The vertical dashed line refers to the interruption during the synthesis. The three lines correspond to the three layers of the alumina support tubes, and the four columns to the different steps in time during synthesis. At t=0, the porous volume is completely filled up by the precursor. After 8-h synthesis, the weight uptake corresponds to a complete depletion of the corresponding amount of precursor due to MFI crystallization. In the course of the interruption (from time 8 to 17 h), the precursor diffuses and is allowed to fill up again the porous network, allowing further crystal growth and eventually support pore plugging with zeolite, but only in the 0.2 μm pore support layer.

Some simple calculations reveal a ~14% plugging of the available pore volume of the alumina top layer by MFI material. This value has been obtained from the total available precursor material present in solution in the top layer successively before and after the interruption. This amount, together with some that might be coming from the precursor diffused into the top layer pores during the whole synthesis process (i.e. 89 h) appears to be sufficient to allow pore plugging. This results in the formation of a thin and continuous nanocomposite material, leading to high separation performance while keeping high permeances (see Fig. 4).

The EDX analyses shown in Fig. 3 reveal the growth of an important amount of MFI material in the first 20-μm depth porous network, involving essentially the 0.2-μm mean pore top-layer of the alumina supports. This result is consistent with the cross-section SEM micrograph obtained at the end of the hydrothermal synthesis (Fig. 2f), where the presence a new material can be distinguished in this layer.

The EDX analyses shown in Fig. 3 reveal the growth of an important amount of MFI material in the first 20-μm depth porous network, involving essentially the 0.2-μm mean pore top-layer of the alumina supports. This result is consistent with the cross-section SEM micrograph obtained at the end of the hydrothermal synthesis (Fig. 2f), where the presence a new material can be distinguished in this layer.

4.2 Effect of the top-layer pore size and material on pore plugging

All the membranes grown on 0.1 and 0.2-μm top layer supports show good quality after full-duration synthesis, achieving *n*-butane/H_2 separation factors in the 30-400 range (see Table 2). Moreover, the gas separation patterns show good reproducibility, as can be inferred from the very similar thermal behaviour (see Fig. 6). This suggests that for these pore-size values, pore plugging is effective. Let us recall that for top layer pore sizes higher than a critical value (0.5 μm, as previously reported [16]), pore plugging is incomplete.

In the case of supports including an additional 5-nm mean pore size γ-alumina layer (see Fig. 6), this layer becomes cracked and partially removed, likely due to the alkalinity of the synthesis medium. In any case, as shown by SEM micrographs, no continuous MFI film is formed neither on the remaining γ-alumina material nor on the liberated α-alumina layer. Even if the resulting membranes showed lower *n*-butane/H_2 separation factors (see Table 2), displaying some membrane defects, these images confirm the presence of a separative nanocomposite zone within the porosity of the alumina support.

Despite the partial leaching of γ-alumina during the synthesis, the weight uptake of the γ-alumina tubes is comparable to that of the other supports (see Table 2). As a matter of fact, a simple calculation reveals that the weight variation corresponding to the disappearance of the whole γ-alumina layer is negligible when compared to that ascribed to MFI formation. This Al-leaching may lead to very high local Al concentrations, which might affect the MFI growth, limiting a complete plugging. This could explain the observed relatively poor separation performance.

4.3 Determination of the effective thickness of nanocomposite membranes

Due the membrane nanocomposite structure, the thickness of the MFI material cannot be inferred from SEM imaging, as is usually the case with film-like membranes. However, a gas-transport effective value can be determined from parameter $\overset{\circ}{D}_{\infty}/\ell$ obtained from the MS fittings, using the value of the diffusivity at zero coverage of the permeating species, $\overset{\circ}{D}_{\infty}$. Nevertheless, the values of these diffusivities might change much depending on the method used for their determination. The diffusivities measured from microscopic methods (PFG-NMR and QENS) correspond in fact to self-diffuvities determined at equilibrium (absence of concentration gradients), while those measured from macroscopic methods (FR, chromatography, MBR/CU) refer to transport diffusivities measured in the presence of concentration gradients.

As an example, Table 4 collects some intrinsic diffusivity values published in the literature for propane in silicalite-1 measured by a number of experimental techniques, which could be further used to calculate an effective thickness. As can be seen, microscopic methods like QENS and PFG-RMN tend to provide much higher diffusivity values than those obtained by macroscpic methods such as ZLC, response frequency (RF) or from diffusion within a silicalite-1 single crystal (SCMBR). It has been traditionally argued that macroscopic techniques provide lower diffusivity values on the grounds of external diffusion limitations, counterdiffusion effects in the case of diluted systems, or defects in zeolite crystals. In contrast, microscopic techniques are not affected by external resistances, since diffusivities are measured from diffusion inside the zeolite crystal and even sometimes only from one adsorption site to the next. The results obtained from molecular modelling (e.g., MD) approach the values measured by microscopic techniques, since the simulations assume implicitly that zeolite crystals are perfect and that intracrystalline mass transfer does not suffer from external resistances.

Table 4.
Intrinsic self- and transport diffusivities of propane in silicalite-1 reported in the literature. In italics, self-diffusivities. In bold, transport diffusivities used for effective thickness estimation

T (K)	Method	Diffusivity (10^{-9} m.s^{-2})	Reference	ℓ computed (μm)
313	NMR	3.9	[33]	16
300	MD	2.0	[34]	9.6
300	QENS	1.2	[35]	5.8
323	**FR**	**0.6**	**[36]**	**2.2**
333	**FR**	**0.5**	**[36]**	**2.0**
334	SCMBR	$7.3.10^{-3}$	[37]	0.02
400	CHTG	$2.9.10^{-6}$	[38]	5.10^{-6}
323	**SCMBR**	**0.38**	**[39]**	**1.4**
323	**SCMBR**	**0.49**	**[40]**	**1.8**
303	ZLC	$7.3.10^{-3}$	[41]	0.03

Nomenclature: MD, Molecular Dynamics; QENS, Quasi-elastic neutron-scattering; SCMBR, Single crystal membrane; CHTG, Chromatography; FR, frequency response; ZLC, zero-length column.

On the basis of the above stated considerations, it seems reasonable to only use transport diffusivities for the calculation of the effective thickness from fitted transport diffusivities. The studies involving the determination of diffusivities from gas permeation within film-like membranes and estimation of the zeolite film thickness microscopy (e.g., [31,32]) have been omitted due to the uncertainty in the determination of the effective thickness by microscopy techniques. Moreover, the modelling behind gas transport in most references is different from that used here (i.e. activation term added to MS equation).

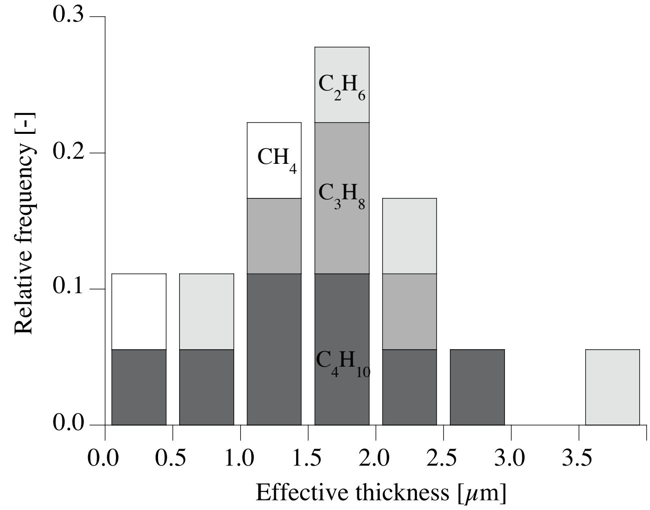

Fig. 8. Relative frequency of the effective thickness of the tested membrane computed using different transport diffusivity values for C1-C4 alkanes.

Fig. 8 plots the distribution of the computed effective thicknesses in the range 0.2-10 μm from parameter D_∞/ℓ obtained from MS fittings of C1-C4 pure alkane permeance using the corresponding published intrinsic transport diffusivities values. Effective thicknesses lower than the mean pore size of the top layer, 0.2 μm, lacking of physical sense, have been disgarded. As can be seen, a higher frequency of values can be found between 0.5-2.5 μm. This is especially the case for ethane and propane. Accordingly, a mean value of 1.5 μm can be chosen for the effective thickness of the tested membrane. It is interesting to note that this value is in fairly good agreement with the minimum pore-volume plugging estimated in section 4.1, i.e. 14%, which corresponds to a thickness about 2 μm. Although this method is of course approximate due to the dispersion of diffusivity values, it provides a quite realistic estimate of the effective thickness of nanocomposite membranes.

It has to be noted that the zeolite membrane is thinner than the support toplayer. One can wonder if both are related. It is possible that deacreasing the support toplayer thickness would provide a mean to decrease the separative thickness. However, within the scope of this work, it is difficult to answer this question.

5 Conclusions

This study points to the role of an interruption during hydrothermal synthesis in the nucleation and crystal growth processes that occur in the support pores during the formation of nanocomposite MFI-alumina material. A 9-h interruption during the synthesis seems to allow nutrient precursor moieties to diffuse into the support pores, further nucleate, crystallize as the synthesis progresses and eventually plug the support pores. As a result, a composite MFI-alumina separative layer is obtained. The supports including top layers of about 0.1 and 0.2-μm pore size allow embedding of the zeolitic material into the support pores.

As opposed to more conventional zeolite membrane synthesis protocols, no continuous and well-intergrown film is formed on top of the support.

In addition, the effective thickness of the equivalent active zeolitic layer was determined (~2 μm) using a method based on gas transport.

6 Acknowledgements

The authors would like to express their gratitude to the European Union for granting projects CT95-0018 ‘Microporous ceramic membranes for gas separation processes’ and G1RD-CT1999-00078 ‘Improved membranes and processes for the low energy recovery of ammonia in synthesis plants’ (Impress). The authors would also like to thank Pall-Exekia for financial and technical support. Y. Li is grateful to the CNRS for an associate researcher grant. M.P-T. thanks the European Union for a Marie Curie EIF grant.

The authors would like to give special thanks to A. Tuel, V. Valtchev and M. Kocirik for fruitful discussion about zeolite synthesis.

7 References

[1] J. Caro, M. Noack, Zeolite membranes – Recent developments and progress, *Micropor. Mesopor. Mater.* **2008** (In Press).

[2] Y. Li, W. Yang, Microwave synthesis of zeolite membranes: a review, *J. Membr. Sci.* **316** (2008) 3.

[3] A. Julbe, Chapter 6 Zeolite membranes – synthesis, characterization and application, *Stud. Surf. Sci. Catal.* **168** (2007) 181.

[4] E.E. McLeary, J.C. Jansen, F. Kapteijn, Zeolite based films, membranes and membrane reactors: Progress and prospects, *Micropor. Mesopor. Mater.* **90** (2006) 198.

[5] T.C. Bowen, R.D. Noble, J.L. Falconer, Fundamentals and applications of pervaporation through zeolite membranes, *J. Membr. Sci*. **245** (2004) 1.

[6] Y.S. Lin, I. Kumakiri, B.N. Nair, H. Alsyouri, Microporous inorganic membranes, *Sep. Purif. Methods* **32** (2002) 229.

[7] J. Coronas, J. Santamaria, Separations using zeolite membranes, *Sep. Purif. Methods.* **28** (1999) 127.

[8] Y. Morigami, M. Kondo, J. Abe, H. Kita, K.-I. Okamoto, The first large-scale pervaporation plant using tubular-type module with zeolite NaA membrane, *Sep. Purif. Technol*. **25** (2001) 251.

[9] Y. Sasaki, W. Shimizu, Y. Ando, H. Saka, Microstructure analysis with TEM for zeolite layer formed in pore of porous alumina substrate, *Micropor. Mesopor. Mater*. **40** (2000) 63.

[10] P.H. Nelson, M. Tsapatsis, S.M. Auerbach, Modeling permeation through anisotropic zeolite membranes with nanoscopic defects, *J. Membr. Sci*. **184** (2001) 245.

[11] M. Pera-Titus, C. Fite, V. Sebastian, E. Lorente, J. Llorens, F. Cunill, Modelling pervaporation of ethanol/water mixtures within ‘real’ zeolite NaA membranes, *Ind. Eng. Chem. Res.* **47** (2008) 3213.

[12] A. Gouzinis, M. Tsapatsis, On the preferred orientation and microstructural manipulation of molecular sieve films prepared by secondary growth, *Chem. Mater.* **10** (1998) 2497.

[13] J. Hedlund, M. Noack, P. Kölsch, D. Creaser, J. Caro, ZSM-5 membranes synthesized without organic templates using a seeding technique, J. Sterte, *J. Membr. Sci.* **159** (1999) 263.

[14] Z. Lai, G. Bonilla, I. Diaz, J.G. Nery, K. Sujaoti, M.A. Amat, E. Kokkoli, O. Terasak, R.W. Thompson, M. Tsapatsis, D.G. Vlachos, Microstructural optimization of a zeolite membrane for organic vapor separation, *Science* **300** (2003) 456.

[15] S. Miachon, I. Kumakiri, P. Ciavarella, L. van Dyk, K. Fiaty, Y. Schuurman, J.-A. Dalmon, Nanocomposite MFI-alumina membranes via pore-plugging synthesis: Preparation and morphological characterisation, *J. Membr. Sci*. **298** (2007) 71.

[16] S. Miachon, E. Landrivon, M. Aouine, Y. Sun, I. Kumakiri, Y. Li, O. Pachtová Prokopová, N. Guilhaume, A. Giroir-Fendler, H. Mozzanega, J.-A. Dalmon, Nanocomposite MFI-alumina membranes via pore-plugging synthesis : Specific transport and separation properties, *J. Membr. Sci.* **281** (2006) 228.

[17] C. Chau, I. Prevost, J.-A. Dalmon, S. Miachon, Preparation of supported zeolitic membranes by temperature-controlled crystallization, US Patent 6,582,495, 24.06.2003.

[18] A. Giroir-Fendler, J. Peureux, H. Mozzanega, J.-A. Dalmon, Characterisation of a zeolite membrane for catalytic membrane reactor application, *Stud. Surf. Sci. Catal.* **101A** (1996) 127.

[19] A. Alshebani, M. Pera-Titus, Th. Schiestel, E. Landrivon, S. Miachon, J.-A. Dalmon, Zeolite hollow fiber ceramic membranes: prospects for CO_2 separation, *Micropor. Mesopor. Mater.* (2008) (In Press).

[20] S. Heng, P.P.S. Lau, K.L. Yeung, M. Djafer, J.-C. Schrotter, Low-temperature ozone treatment for organic template removal from zeolite membrane, *J. Membr. Sci.* **243** (2004) 69.

[21] J. Hedlund, F. Jareman, A.-J. Bons, M. Anthonis, A masking technique for high quality MFI membranes, *J. Membr. Sci.* **222** (2003) 163.

[22] J. Dong, Y.S. Lin, M.Z.-C. Hu, R.A. Peascoe, E. Paysant, Template-removal-associated microstructural development of porous-ceramic-supported MFI zeolite membranes, *Micropor. Mesopor. Mater.* **34** (2000) 241.

[23] L. van Dyk, L. Lorentzen, S. Miachon, J.-A. Dalmon, Xylene isomerization in an extractor type catalytic membrane reactor, *Catal. Today* **104** (2005) 274.

[24] O. Camus S. Perera, B. Crittenden, Y.C.V. Delft, F. Dick, P. Meyerb, P.A.C. Pex, I. Kumakiri, S. Miachon, J.-A. Dalmon, S. Tennison, Ph. Chanaud, Ceramic membranes for ammonia recovery, *AIChE J.* **52** (2007) 2055.

[25] P. Ciavarella, D. Casanave, H. Moueddeb, S. Miachon, K. Fiaty, J.-A. Dalmon, Isobutane dehydrogenation in a membrane reactor. Influence of the operating conditions on the performance, *Catal. Today* **67** (2001) 177.

[26] S. Miachon, A. Mazuy, J.-A. Dalmon, Catalysis of palladium salt reduction in a gas-liquid membrane reactor, *Stud. Surf. Sci. Catal.* **130** (2000) 2693.

[27] B. Hamad, A. Alshebani, M. Pera-Titus, B. Albela, L. Bonneviot, S. Miachon, J.-A. Dalmon, Synthesis and characterization of nanocomposite MCM-41 ('LUS')–tubular membranes, *Micropor. Mesopor. Mater.* (2008) (In Press).

[28] P. Ciavarella, H. Moueddeb, S. Miachon, K. Fiaty, J.-A. Dalmon, Experimental study and numerical simulation of hydrogen/isobutene permeation and separation using MFI-zeolite membrane reactor, *Catal. Today* **56** (2000) 253.

[29] A. Alshebani, M. Pera-Titus, K.L. Yeung, S. Miachon, J.-A. Dalmon, Influence of pre-treatment on the *n*-butane/hydrogen separation performance of nanocomposite MFI zeolite membranes, *J. Membr. Sci*. **314** (2008) 143.

[30] C.S. Cundy, P.A. Cox, The hydrothermal synthesis of zeolites: precursors, intermediates and reaction mechanism, *Micropor. Mesopor. Mater.* **82** (2005) 1.

[31] W.J.W. Bakker, L.J.P. van den Broeke, F. Kapteijn, J.A. Moulijn, Temperature dependence of one-component permeation through a silicalite-1 membrane, *AIChE J.* **43** (1997) 2203.

[32] F. Kapteijn, W.J.W. Bakker, G. Zheng, J.A. Moulijn, Temperature- and occupancy-dependent diffusion of n-butane through a silicalite-1 membrane, *Micropor. Mater.* **3** (1994) 227.

[33] J. Caro, M. Buelow, W. Schirmer, J. Kärger, W. Heink, H. Pfeifer, Microdynamics of methane, ethane, and propane in ZSM-5 type zeolites, *J. Chem. Soc. Faraday Trans.* **81** (1985) 2541.

[34] J.B. Nicholas, F.R. Trouw, J.E. Mertz, L.E. Iton, A.J. Hopfinger, Molecular dynamics simulation of propane and methane in silicalite, *J. Phys. Chem.* **97** (1993) 4149.

[35] H. Jobic, M. Bée, G.J. Kearley, Dynamics of ethane and propane in zeolite ZSM 5 studied by quasi-elastic neutron scattering, *Zeolites* **12** (1992) 146.

[36] N. van den Begin, L.V.C. Rees, Fast adsorption-desorption kinetics of hydrocarbons in silicalite-1 by the single-step frequency response method, *Zeolites* **9** (1989) 287.

[37] D.T. Hayhurst, A.R. Paravar, Diffusion of C1 to C5 normal paraffins in silicalite, *Zeolites* **8** (1988) 27.

[38] A.S. Chiang, A.G. Dixon, Y.H. Ma, The determination of zeolite crystal diffusivity by gas chromatography - II. Experimental, *Chem. Eng. Sci.* **39** (1984) 1461.

[39] O. Talu, M.S. Sun, D.B. Shah, Diffusivities of n-alkanes in silicalite by steady-state single-crystal membrane technique, *AIChE J.* **44** (1998) 681.

[40] M.S. Sun, O. Talu, D.B. Shah, Diffusion measurements through embedded zeolite crystals, *AIChE J.* **42** (1996) 3001.

[41] M. Eic, D.M. Ruthven, Intracrystalline diffusion of linear paraffins and benzene in silicalite studied by the ZLC method, in: P.A. Jacobs, R.A. van Santen (Eds.), Proceedings of the 8th International Conference on Zeolites, Elsevier, Amsterdam, 1989, p. 897.